PCCP

Rational Design of Solid-Acid Catalysts for Cellulose Hydrolysis Using Colloidal Theory

Journal:	*Physical Chemistry Chemical Physics*
Manuscript ID	CP-ART-01-2021-000198.R1
Article Type:	Paper
Date Submitted by the Author:	30-Mar-2021
Complete List of Authors:	Zhang, Ziyang; Worcester Polytecchnic Institute, Chemical Engineering Tompsett, Geoffrey; Worcester Polytecchnic Institute, Chemical Engineering Lambert, Christopher; Worcester Polytchnic Institute, Bioengineering Institute Granados-Focil, Sergio; Clark University, Gustaf Carlson School of Chemistry and Biochemistry Timko, Michael; Worcester Polytecchnic Institute, Chemical Engineering

ARTICLE

Rational Design of Solid-Acid Catalysts for Cellulose Hydrolysis Using Colloidal Theory

Received 00th January 20xx,
Accepted 00th January 20xx

DOI: 10.1039/x0xx00000x

Ziyang Zhang, [a] Geoffrey A. Tompsett, [b] Sergio Granados-Focil, [c] Christopher R. Lambert, [d] Michael T. Timko [e]

Solid-acid catalysts functionalized with catalytic groups have attracted intense interest for converting cellulose into soluble products. However, design of solid-acid catalysts has been guided by molecular level of interactions and the actual mechanism of cellulose-solid-acid catalyst particles adsorption remains unknown. Here, colloidal stability theory, DLVO, is used to rationalize the design of solid acids for targeted cellulose adsorption. In nearly all cases, an energy barrier, arising from electrostatic repulsion and much larger than the energy associated with thermal fluctuations, prevents close contact between the solid acid and cellulose. Polymer-based solid-acid substrates such as polystyrene and Nafion are especially ineffective as their interaction with cellulose is dominated by the repulsive electrostatic force. Carbon and metal oxides have potential to be effective for cellulose-solid-acid interaction as their attractive van der Waals interaction can offset the repulsive electrostatic interaction. The effects of reactor temperature and shear force were evaluated, with the finding that reactor temperature can minimize the catalyst-cellulose interaction barrier, promoting coagulation, but that the shear force in a typical laboratory reactor cannot. We have evaluated strategies for enhancing cellulose-catalyst interaction and conclude that raising reaction temperature or synthesizing acid/base bifunctional catalysts can effectively diminish electrostatic repulsion and promote cellulose-catalyst coagulation. The analysis presented here establishes a rational method for designing solid acid catalysts for cellulose hydrolysis.

1. Introduction

Cellulose is the most abundant source of renewable carbon on the planet, and its deconstruction is a key step for decarbonizing an economy that relies on petrochemicals and petroleum fuels.[1-3] Liquid acid pre-treatment followed by enzymatic hydrolysis is the most commercially advanced technology for converting biomass into simple sugars[4-6]. However, the process remains economically unfeasible because of the costs associated with acid, product recovery, and enzymes.[7, 8]

Solid-acid catalysts have recently been proposed as alternatives to the liquid acids used for biomass deconstruction because they can be recovered and reused, with subsequent cost reductions over their lifetime.[9-11] Moreover, some reports suggest that solid-acids make possible direct and selective conversion of cellulose into glucose under mild conditions.[9] Accordingly, the number of published articles mentioning the key words “solid-acid” and “cellulose hydrolysis” has exploded from <10 before 2008 to more than 500 in 2019 (see Figure SI-1).

In most cases, solid-acid catalysts have been used in aqueous mixtures, meaning that both the feed and the solid-acid catalyst itself are present as solid particles before and after the reaction.[9] The presence of both the catalyst and the substrate as solid particles leaves open the question of how the catalyst and substrate can remain close enough together for time scales sufficient for reaction to occur. Several theories seek to explain the mechanism on the molecular level, suggesting that favorable hydrogen bonding, London dispersion or CH-π interactions are responsible for cellulose-solid-acid binding that allows for reaction of catalytic groups with cellulose’s glycosidic bonds, implicating a solid-solid catalytic mechanism that has not yet been tested directly.[12] Some of these explanations explicitly invoke the binding module of cellulase that uses various dispersion interactions to target the enzyme to hydrolysable bonds.[13, 14]

Despite its apparent popularity, the molecular-level theory of solid-acid binding to cellulose has major flaws. First, as demonstrated by Tyufekchiev *et al.*,[15] the binding theory does not capture the important role played by release of soluble acids by the solid catalyst

[a] Department of Chemical Engineering, Worcester Polytechnic Institute, 100 Institute Road, Worcester MA 01609, United States. Email: zzhang10@wpi.edu
[b] Department of Chemical Engineering, Worcester Polytechnic Institute, 100 Institute Road, Worcester MA 01609, United States. Email: gtompsett@wpi.edu
[c] Department of Chemistry, Clark University Worcester, MA 01610, United States. Email: sgranadosfocil@clarku.edu
[d] Department of Chemistry & Biochemistry, Worcester Polytechnic Institute, 100 Institute Road, Worcester MA 01609, United States. Email: clambert@wpi.edu
[e] Department of Chemical Engineering, Worcester Polytechnic Institute, 100 Institute Road, Worcester MA 01609, United States. Email: mttimko@wpi.edu

during its degradation under reaction conditions. These soluble acids then are responsible for the majority of the observed hydrolysis activity, meaning that the solid-acid becomes – in effect – a very expensive way to deliver liquid acid to the reaction mixture. Second, and more fundamentally while molecular-level interactions may explain the ability of cellulase to target glycosidic bonds, there is a problem of length scale for solid-acids. Whereas cellulase is a nanoparticle with characteristic length of several nanometers, [16] the characteristic lengths of most solid-acid catalysts used for cellulose hydrolysis are usually >1 μm.[17] Applying molecular-level explanations to nano-scale enzymes stretches the limits of interaction theory; applying these same explanations to microparticles is clearly insufficient. [18]

Instead of molecular theories, catalyst-cellulose interactions should be more properly analyzed using colloidal theories to enable rational catalyst design. Colloidal particles interact with one another *via* van der Waals, electrical double layer, hydrophobic, hydration, and steric forces. Of these, van der Waals and electrical double layer forces are present in all colloidal interactions, whereas the others are important only in specific situations.[19] Quantitatively, DLVO theory, named after its creators Boris Derjaguin, Lev Landau, Evert Verwey and Theodoor Overbeek,[20] describes the overall particle-particle interaction (U) as the sum of van der Waals (U_{VDW}) and electrical double layer forces (U_{EDL}) thereby offering a logical starting point for colloidal-level analysis of solid-acid catalyzed hydrolysis of biomass polymers.

In this work, we applied colloidal-level DLVO theory to study the interaction of cellulose micro-particles with various solid-acid catalysts, including activated carbon, iron oxide (Fe_3O_4), zirconia (ZrO_2), polystyrene and Nafion. DLVO models used reported zeta potential at different pH and Hamaker constants to estimate the maximum energy barrier (U_{max}) that catalyst particles must surmount before coagulating with cellulose and reacting. We then use the energy calculations as a guide to evaluate strategies for promoting cellulose-solid-acid catalyst interactions. The analysis presented here can help guide future rational design of solid acid catalysts for cellulose hydrolysis.

2. Theory

2.1 DLVO

The DLVO interaction energy between cellulose and solid-acid consists of van der Waals and electrical double layer forces, which can be written: [18]

$$U = U_{VDW} + U_{EDL} \quad (1)$$

where U_{VDW} and U_{EDL} denote van der Waals attraction and electrostatic repulsion respectively. The van der Waals energy (U_{VDW}) was derived as: [18]

$$U_{VDW} = -\frac{A_{132}}{6}\left[\frac{2r_1r_2}{x(2r_1+2r_2+x)} + \frac{2r_1r_2}{(2r_1+x)(2r_2+x)} + \ln\frac{(2r_1+2r_2+x)x}{(2r_1+x)(2r_2+x)}\right] \quad (2)$$

where r_1 and r_2 are radius of cellulose and catalyst; A_{132} is the combined Hamaker constant for cellulose ("1")-solid-acid catalyst ("2") interaction across water ("3"). Hamaker constant is typically determined by Lifshitz' s combining rule that is: [21]

$$A_{132} = -\left(\sqrt{A_{11}} - \sqrt{A_{33}}\right)\left(\sqrt{A_{22}} - \sqrt{A_{33}}\right) \quad (3)$$

where A_{11}, A_{22} and A_{33} denote cellulose, solid-acid catalyst and water interacting with itself in vacuum. For individual Hamaker constant, Lifshitz' s quantum theory can be used to determine them separately based on: [21]

$$A_{ii} = \frac{3}{4}k_bT\left(\frac{\varepsilon_i+1}{\varepsilon_i-1}\right)^2 + \frac{3h\nu_e}{16\sqrt{2}}\frac{(n_i^2-1)^2}{(n_i^2+1)^{3/2}} \quad (4)$$

where ν_e is the main electronic absorption frequency in the ultraviolet region, typically around 3×10^{15} s^{-1}.

Electrical double layer repulsion (U_{EDL}) can be derived from the Poisson-Boltzmann (P.B.) distribution given by [22]

$$\nabla^2\psi = \frac{8\pi cez}{\varepsilon_0\varepsilon_3}\sinh\left(\frac{ze\psi}{k_bT}\right) \quad (5)$$

For spherical particles with dissimilar radius and surface charge density, the P.B. can be integrated and simplified as the following:

$$U_{EDL}(x) = \frac{\varepsilon_0\varepsilon_3 r_1 r_2(\psi_{01}^2+\psi_{02}^2)}{4(r_1+r_2)}\left[\frac{2\psi_{01}\psi_{02}}{(\psi_{01}^2+\psi_{02}^2)}\ln\left(\frac{1+\exp(-\kappa x)}{1-\exp(-\kappa x)}\right) + \ln(1-\exp(-2\kappa x))\right] \quad (6)$$

where ψ_{01} and ψ_{02} are surface potential of cellulose and catalyst respectively; κ is the Debye length.

2.2 Bifunctional catalyst surface potential model

For a bifunctional solid-acid catalyst, experimental ζ measurements are typically not available, a new model is needed to relate surface acid density and dissociation constant to surface potential.[23] For a bifunctional catalyst bearing acid groups (*AH*) and base groups (*BOH*), the surface can be charged through deprotonation of *HA* and protonation of *BOH*:

$$AH \rightleftarrows H^+ + A^-$$
$$BOH \rightleftarrows OH^- + B^+$$

Two assumptions can be applied to simplify the model: i) ionization of individual sites are independent of one another and do not interact with each other; ii) protonation of *HA* occurs only under extremely acidic condition (typically *pH* < 1,) that are not of interest here. The consequence of these two assumptions is that the Ka of the bound acid is the same as the free version, which may not necessarily be valid for conditions of high surface density.[24]

With these two assumptions, dissociation can be quantified by the appropriate equilibrium constant (either *Ka* or K_b):

$$K_a = \frac{[H^+]_0\Gamma_{A^-}}{\Gamma_{AH}} \quad (7)$$

$$K_b = \frac{[OH^-]_0 \Gamma_{B^+}}{\Gamma_{BOH}} \quad (8)$$

where $[H^+]_0$ is the protons activity around solid-acid catalyst surface and $[OH^-]_0$ is the hydroxide ions activity around surface. Γ_{AH} is surface acid density for undissociated acid and Γ_{A^-} is the surface density for dissociated acid or substrate catalyst, and the same definition applies to *BOH*.

Applying the P.B. distribution equation, the proton activity around the solid surface and that in bulk phase can be correlated as: [23]

$$[H^+]_0 = [H^+]_b ex\, p\left(-\frac{e\psi_0}{k_b T}\right) \quad (9)$$

When placed in a solution with *pH* > pKa, the surface will become negatively charged, resulting in a non-zero value of the surface charge density (σ_0):[23]

$$\sigma_0 = eN_A \{\Gamma_{B^+} - \Gamma_{A^-}\} \quad (10)$$

The surface acid coverage can then be related to the dissociated acid surface concentration. The total acid concentration consists of dissociated and undissociated site density for both acid head group and substrate catalysts and is given by:

$$\Gamma_{A_t} = \Gamma_{AH} + \Gamma_{A^-} \quad (11)$$

$$\Gamma_{B_t} = \Gamma_{BOH} + \Gamma_{B^+} \quad (12)$$

Equations (7-12) can be solved for surface charge density as a function of measurable quantities, including *pH*, *pKa*, surface coverage (Γ_{tot}). However, upon solving the above equations, surface charge density and surface potential are inter-correlated. Obtaining separate equations for surface potential and density individually requires a separate equation. Here, the Grahame equation will be used to relate surface charge density to surface potential, since it is appropriate for curved surfaces: [25]

$$\sigma_0 = \frac{\varepsilon_0 \varepsilon_3 \kappa k_b T}{2\pi e}\left[\sinh\left(\frac{e\psi_0}{2k_b T}\right) + \frac{2}{\kappa a}\tanh\left(\frac{e\psi_0}{4k_b T}\right)\right] \quad (13)$$

Solving Equations (7-13) simultaneously allows explicit determine of either the surface potential (ψ_0) or surface charge density (σ_0).

3. Results and Discussions

The design of solid-acid for hydrolyzing cellulose has long been guided by molecular interaction. However, given that both cellulose and catalyst are present as solid before and after the reaction, DLVO theory must be used to rationalize catalyst design. Figure 1a and Figure 1b are schematic representations of the particle-particle interaction predicted by DLVO theory (top panel) and the resulting colloidal suspensions (bottom panel), shown both for particles with similar (Figure 1a) and dissimilar charges (Figure 1b).

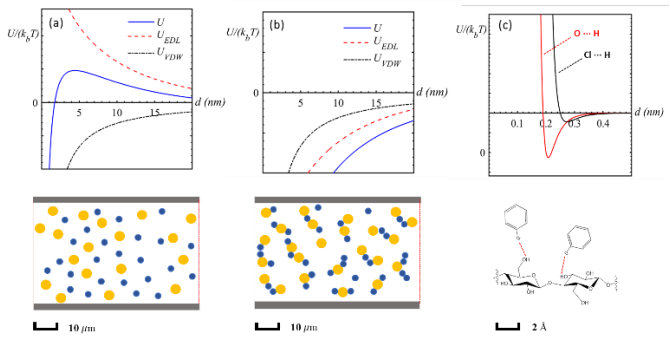

Figure 1. Schematics of particle-particle interactional energy as functions of particle separation (yellow sphere represents cellulose and blue sphere represents solid-acid catalyst: (a) like-charge colloidal interactional energy as function of particle separation, (b) unlike-charge colloidal interaction as function of separation, (c) approximated single hydrogen bonding interaction energy between cellulose chain and chlorobenzene. Note that the *x*-axis scale is 20 nm in Figure 1a and Figure 1b and 0.5 nm in Figure 1c.

In the case of particles with similar charges, particles must surmount an energy barrier located several nanometers from the particle surface before they can interact. Crucially, the location of the barrier (>1-3 nm separation) is far beyond the range of molecular non-bond interaction such as hydrogen bonds (<2 Å), meaning that macro-particles should overcome the energy barrier caused by DLVO effect before hydrogen bonds or other forms of van der Waals interaction can be formed between particles. At best, catalyst particles might interact at a distance with cellulose, for example by water mediated proton transfer;[26] however, decreasing the separation distance less than 10 nm incurs an increasing energy penalty that opposes such interaction.

The bottom panels of Figure 1 are particle-particle schematics. The net repulsive energy barrier predicted for similarly charged particles results in stable dispersions (Figure 1a, bottom panel). For dissimilarly charged particles, the net interaction is attractive, resulting in fast-coagulation (Figure 1b, bottom panel). For catalytic applications, coagulation is the desired outcome. That stated, catalyst particles bearing acid groups will invariably be negatively charged in solution. So, too, are cellulose particles. Accordingly, acid catalysts and cellulose are predicted to form stable colloids, rather than undergoing coagulation.

For comparison, Figure 1c is a molecular-level schematic representation of the interaction energy between a hydrogen bond donor (polysaccharide) and acceptor (chlorobenzene), the suggested interaction responsible for particle-particle catalysis. Unlike Figure 1a and 1b, Figure 1c shows that molecules or atoms experience no interaction barrier aside from the extremely short range (<1 Å) steric interaction. For similarly charged particles the situation is qualitatively different, and Figure 1 makes clear that applying molecular level explanations to colloidal phenomena, as has been done for solid-acid catalysis of cellulose, is insufficient.

The objective for catalysis is to design an “unstable dispersion” that encourages catalyst-cellulose interaction. Colloidal theory can be used for designing solid-acids for which the repulsive barrier for

interacting with cellulose is <25 k_bT, an arbitrary value but one that is based on empirical observations of colloidal stability.[27] Ideally, this interaction could be tuned by changing *pH*, ionic strength, or temperature; accordingly, the solid catalyst could be used under one set of conditions for cellulose hydrolysis. Clearly, this level of manipulation is not possible without a firm scientific basis and theoretical analysis, which is what this work aims to develop.

For spherical particles, the DLVO equation can be reduced to a function of particle diameter, solution phase *pH*, ionic strength, Debye length, and a collection of parameters that are known or can be estimated for cellulose and many important solid-acid catalyst types, including inorganic materials, polymeric, and functionalized carbons.[18] The SI contains the details on how DLVO theory was applied to the catalyst-cellulose problem. The most important parameter affecting U_{VDW}, aside from particle diameter, is the Hamaker constant, A_{132}. The Hamaker constant depends on the catalyst material and values for several important catalyst materials interacting with cellulose across water are provided in Table 1. Similarly, for U_{EDL}, the most important parameter is the surface potential (ψ). As described in the SI, the surface potential is not typically known. However, the surface potential can be estimated from experimental measurements of the zeta potential (ζ) or estimated from known values of surface acid density, ionic strength, and acid strength (pK_A). Table 1 provides some representative values of zeta potential representative catalyst materials at *pH* values of 1.0, 3.0, and 5.0, as reported in the literature.

Catalyst	Modifier acid	A_{132} ($\times 10^{-21}$ J)	ζ (mV)			Ref.
			pH=1	*pH=3*	*pH=5*	
Cellulose	-	-	-16	-25	-27	[28]
[a] Carbon	Nitric acid	36.0	-30	-37	-40	[29]
[b] Fe_3O_4	Sulfonic acid	35.0	-	-40	-63	[30]
[c] ZrO_2	Citric acid	28.8	-	-18	-42	[31]
[d] Polystyrene	Acrylic acid	10.7	-	-28	-45	[32]
[e] Nafion	-	1.70	-	-45	-70	[33]

Table 1. Hamaker constants and reported zeta potential for representative solid-acid catalysts interacting with cellulose

Note: [a,b,c,d,e] zeta potential at *pH* =1 is not reported; [e] zeta potential for bear Nafion without acid functionalization.

Table 1 defines ranges of the Hamaker constant and surface potential for cellulose and commonly used solid-acids. Cellulose is used as a representative biomass constituent, and the subject of many previous studies of solid-acid catalysis.[9] Figure 2 shows energy-distance curves predicted by Equation (1) for values of the Hamaker constant and surface potential that span the range expected from Table 1, with other factors held constant at representative values (*pH* = 5, fixed catalyst diameter of 1 μm and fixed cellulose particle diameter of 5 μm). Clearly, in most cases, a solid-acid particle will experience a barrier ranging from 10 k_bT to 200 k_bT as it approaches the cellulose surface. Carbon is an exception, due to its large Hamaker constant (Table 1). Inorganic oxides and especially polymers experience a prohibitively large repulsive barrier for interaction with cellulose.

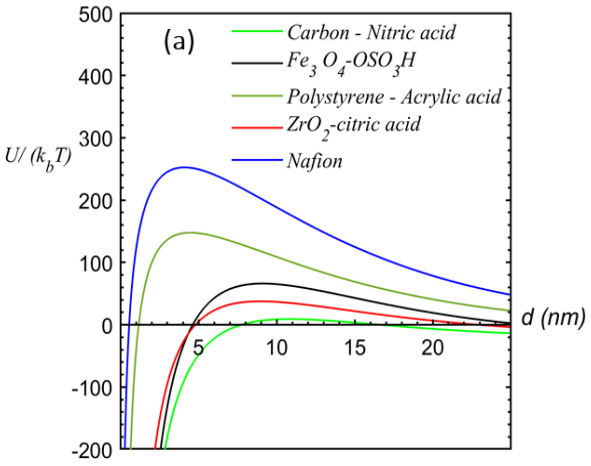

Figure 2. DLVO interaction energy as a function of cellulose-catalyst separation for reported catalysts at *pH* = 5.

A problem with existing catalyst strategies is that partial de-protonation of the acid surface results in a negative surface potential (Table 1). Since cellulose possesses a negative surface potential at *pH* above 2 (Table 1), the resulting U_{EDL} often results in a repulsive barrier preventing catalyst-cellulose interaction, as shown in Figure 2. Keeping the catalyst protonated, by lowering *pH* is one way to avoid the negative surface charge, as shown in a contour plot of energy barrier as a function of $pK_A - pH$ (Figure 3) for representative values of the Hamaker constant (2×10^{-20} J) and acid density (5 nm^{-2}). Figure 3 shows that adjusting *pH* can effectively remove the catalyst-cellulose interaction barrier. However, the problem with acidifying the *pH* is that it requires addition of homogeneous acid, the very problem that was to be solved. For example, reducing the barrier to less than 200 k_bT for a catalyst with pK_A < 2 requires reducing the *pH* to less than 1.1.

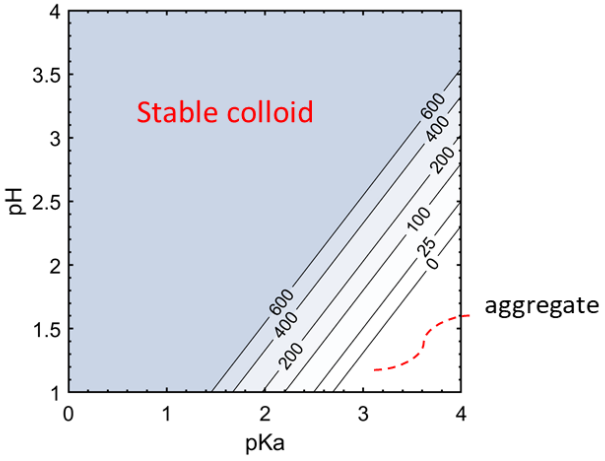

Figure 3. DLVO maximum energy barrier as a function of acid group *pKa* and solution *pH*, assuming acid head group density of 5 nm^{-2}, Hamaker constant of 2×10^{-20} J.

An approach that does not depend on addition of liquid acids is selecting the catalyst material to maximize U_{VDW}. Figure 4 plots the energy barrier as a function of Hamaker constant for three representative values of the surface potential and shows how this approach might work. Hamaker constants of representative materials are superimposed on the plot for reference. Maximizing the Hamaker constant, for example by using carbon-based or inorganic catalyst particles such as zirconia or iron oxide, has potential to reduce the particle-particle interaction barrier to <25 k_bT at surface potential around – 35 mV. In contrast, polymer-based catalysts such as Nafion and polystyrene do not interact with cellulose without a substantial >25 k_bT barrier under any realistic conditions.

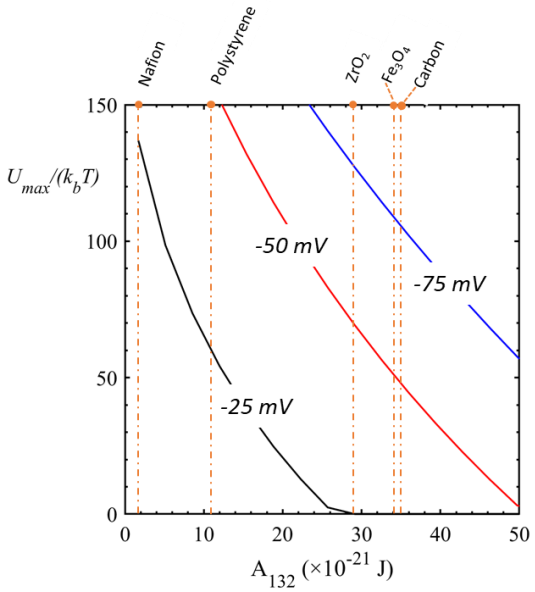

Figure 4. The DLVO energy barrier height as function of Hamaker constant for different values of the surface potential.

Heating the reaction system to 140 – 170 °C is commonly described in the literature for decomposing cellulose under mild conditions.[34] The change of Hamaker constant is around 3% upon raising the temperature from 25 °C to 150 °C.[35] The change of temperature mainly affects dielectric constant and hence the Debye length of the reaction system. Figure 5 shows that increasing temperature to 150 °C may enhance carbon and zirconia-based catalysts ability to adsorb cellulose. Polymer based catalysts such as polyelectrolyte still lack the capacity to interact with cellulose under intermediate temperature.

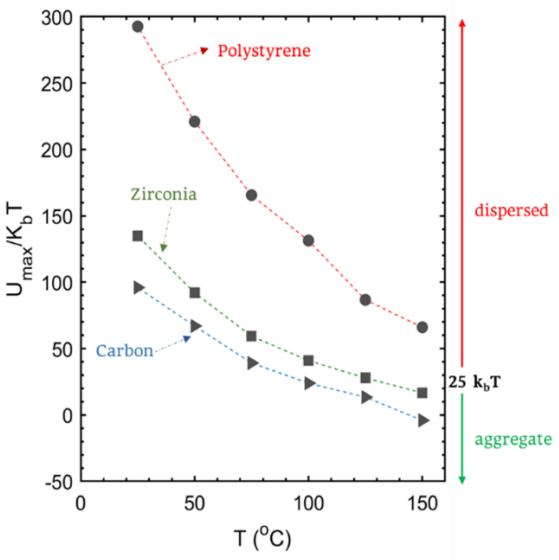

Figure 5. DLVO energy barrier as a function of temperature for cellulose interacting with polystyrene, zirconia, and carbon catalysts. The cellulose diameter is assumed as 5 μm. The surface potential for the catalyst is assumed to be −30 mV and catalysts surface potential are assumed to be – 50 mV.

A final option is the use of a bifunctional catalyst consisting of acid and base groups, which has been successfully synthesized.[36-39] The need for the acid group is clear from the application. However, as shown previously in Figure 2, acid group dissociation leads to the catalyst acquiring a negative charge that then repels the negatively charged cellulose substrate. The role of the base therefore is to balance the negative charge of the partially dissociated acid. Naturally, a bifunctional catalyst must be designed carefully so that the acid and base groups do not simply react in solution to form the corresponding salt. Polyions are an example.[40, 41] Indeed, polyionic materials have been used previously to promote cellulose flocculation,[42] and several solid-acid catalysts proposed for cellulose hydrolysis have possessed cationic groups, including imidazolium,[43] previous work on acidic polymers bearing imidazolium groups have again focused on molecular-level effects, for example using as inspiration the observation that some imidazolium-based ionic liquids are effective cellulose solvents.[43] Here, a colloidal perspective is advocated.

Equation (1) can be used to model the effects of bifunctional catalysts on cellulose binding, using a procedure similar to that adopted to construct Figure 3; the Supporting Information provides details. Figure 6 provides particle-particle interaction curves for representative values of the density of acid to base sites at fixed Hamaker constants characteristic of inorganic solids (2×10^{-20} J), with cellulose particle diameter of 5 μm, catalyst diameter of 1 μm, a *pH* of 5. Figure 6 shows that a bifunctional catalyst can reduce the particle-particle interaction barrier to < 10 k_bT for values of the acid to base density ratio less than or equal to 1. In fact, for the case in which the base site density is twice that of the acid site density, the catalyst-cellulose interaction is attractive at all separations, meaning

that a mixture of that bifunctional catalyst and cellulose may spontaneously coagulate.

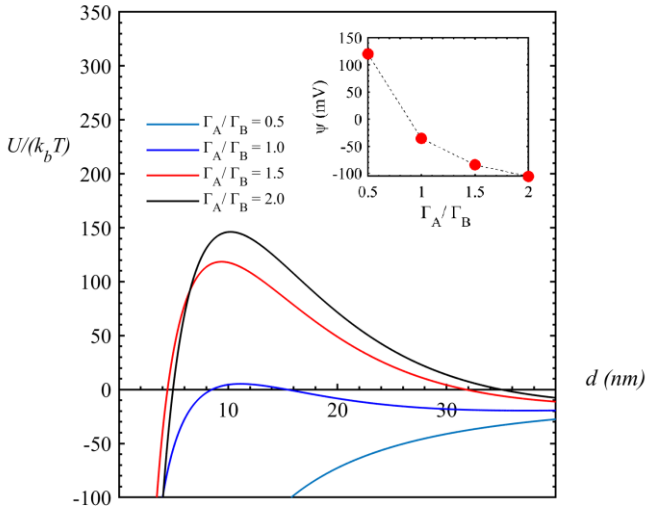

Figure 6. Interaction energy of cellulose with bifunctional catalysts having different ratio of acid to base site density, assuming pK_a as 1 and pK_b as 5.75, total site density Γ_{tot} as 5 nm^{-2}.

For biomass hydrolysis using tightly bound bifunctional catalysts, recovering the catalyst after reaction may pose a challenge.[44] Colloidal-level analysis suggests several recovery strategies. Following with the theme of bifunctional catalysts, *pH* might be used to tune between attractive and repulsive interactions. Accordingly, the reaction might be performed at mildly acidic *pH*, at which conditions the base is protonated, and the catalyst recovered by adjusting the *pH* to de-protonate the base. As with performing the reaction at $pH < pK_A$, which is a viable strategy for promoting catalyst-cellulose aggregation (Figure 3), the *pH* adjustment approach must use small enough quantities of acids and bases not to offset the benefits of catalyst recovery. Similarly, adjusting the temperature might provide a method for catalyst recovery. The theoretical analysis presents calculations performed at room temperature, and the effect of temperature is provided in the SI. As a further option, non-aqueous solvents or solvent mixtures might be considered. The SI provides guidance on the effects of non-aqueous solvents on particle-particle interactions.

The previous discussion has neglected non-DLVO effects, generally categorized as steric, hydration, hydrophobic and shear forces.[18] Of these, cellulose and catalyst particles will both be hydrophilic, meaning that hydrophobic forces can be neglected.[18] Steric forces do not contribute to cellulose-solid-acid interaction aggregation but instead is typically repulsive and can cause stabilization,[45] which is not desirable. Magnitudes of hydration forces are difficult to predict [46] but tend to be important only at length scales much less than the repulsive barrier shown for many situations in cellulose-catalyst interaction in Figure 2. Accordingly, non-DLVO forces are unlikely to play a critical role in catalyst-cellulose interactions for catalysts described in the literature.

In addition to catalyst design, reactor design can be optimized for catalyst-cellulose interaction. Here, shear-force-induced aggregation is an industrially implementable strategy. The SI provides theoretical details of the shear force analysis, reported by Zaccone et al. as an extension of the two-body Smoluchowski equation.[47] The analysis predicts a critical value of the shear rate ($\dot{\gamma}^*$) that, when exceeded, shear forces overcome the repulsive barrier associated with electrostatic interaction, permitting coagulation of particles that DLVO theory predicts would otherwise remain separate.

Figure 7 is a plot of predicted values of the critical shear rate required to coagulate solid acids with varying surface potential and fixed Hamaker constant with cellulose. As expected from the previous discussion, the value of the critical shear rate ($\dot{\gamma}^*$) increases rapidly as catalyst surface potential becomes increasingly negative. Even for mildly negatively charged catalyst with surface potential of approximately -50 mV, as indicated by the horizontal line on Figure 7, $\dot{\gamma}^*$ ranges from 32 s^{-1} to 126 s^{-1}, depending on the catalyst size.

Interpreting Figure 7 requires estimates of shear rates employed in a typical experiment. Most experiments on solid acid hydrolysis of cellulose are reported in glass vials agitated by PTFE® stir bars,[9, 48] conditions that are designed to distribute heat and not for imparting shear. Nonetheless, the maximum shear rate encountered in the glass-vial reactors can be estimated using simple physical principles, as outlined in the SI. The shear rate analysis predicts that a PTFE® stir bar can impart shear rates that range from 2.5 s^{-1} for a stirring rate equal to 200 rpm to 9 s^{-1} at 800 rpm.[15, 49, 50] This range is much less than that predicted for $\dot{\gamma}^*$, as shown in Figure 7. As an alternative, reactors designed for high-shear mixing, potentially using ultrasound or cavitation,[51-53] may achieve localized shear rates sufficient to induce catalyst-cellulose coagulation.

Figure 7 shows predictions for a range of particle size, apparently suggesting that shear-induced coagulation may be a viable approach for particles of sufficient size. This conclusion is likely erroneous given that the assumptions underlying the theory break down as gravity forces become important.[54] Nonetheless, the dependencies of $\dot{\gamma}^*$ and coagulation rate on particle size have been discussed in the literature, suggesting that large particles (a few microns) coagulate at values of $\dot{\gamma}^*$ less than those required for small particles (a few hundred nanometers).[47, 55] That stated, the strategy of using large catalyst particles to exploit shear-induced coagulation has practical limitations as the DLVO coagulation barrier is size dependent,[56] catalytically available surface area is maximized for small particles, and gravity forces become increasingly important as particle size increases, complicating the analysis.[57, 58] In practice, using micron-sized catalyst particles with modest surface potentials in high-shear reactors is more likely to be successful for promoting catalyst-cellulose interactions than using larger catalysts.

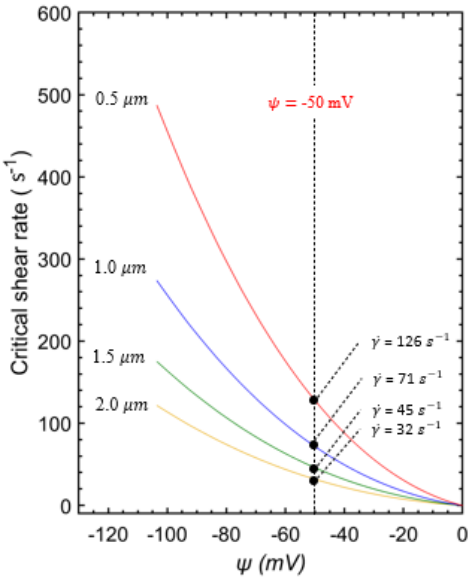

Figure 7. Critical shear rate ($\dot{\gamma}^*$) as a function of catalyst surface potential, assuming catalyst Hamaker constant is 2×10^{-20} J; cellulose surface potential is -27 mV; cellulose diameter is 1 μm.

4. Conclusions

Solid-acids have potential to reduce the costs of producing simple sugars from cellulose-rich biomass. However, work in this field has been falsely guided by molecular-level explanations.[10, 13, 14] Colloidal-level considerations suggest point to new strategies for the design of cellulose-deconstruction solid-acid catalysts. The Hamaker constant must be maximized, particle size should be reduced as much as possible while permitting catalyst recovery, and repulsive forces originating from the electrical double layer must be minimized. Carbon-based or inorganic catalysts with bifunctional acid/base surface groups may be especially effective at meeting these requirements as carbon possesses a favorable Hamaker constant and base groups can neutralize the negative charge that acid groups confer to the catalyst surface. High shear rate is recommended for counterbalancing DLVO repulsive energy barriers and hence promote cellulose-solid acid catalyst coagulation.

Conflicts of interest

There are no conflicts to declare.

Acknowledgements

The U.S. National Science Foundation (ENG #1554283) funded this work.

References

1. Centi, G. and R.A. van Santen, *Catalysis for renewables: from feedstock to energy production*. 2008: John Wiley & Sons.
2. Shen, D., et al., *The pyrolytic behavior of cellulose in lignocellulosic biomass: a review.* RSC advances, 2011. **1**(9): p. 1641-1660.
3. Leschine, S.B., *Cellulose degradation in anaerobic environments.* Annual review of microbiology, 1995. **49**(1): p. 399-426.
4. Humbird, D., et al., *Process design and economics for biochemical conversion of lignocellulosic biomass to ethanol: dilute-acid pretreatment and enzymatic hydrolysis of corn stover*. 2011, National Renewable Energy Lab.(NREL), Golden, CO (United States).
5. Mansfield, S.D., C. Mooney, and J.N. Saddler, *Substrate and enzyme characteristics that limit cellulose hydrolysis.* Biotechnology progress, 1999. **15**(5): p. 804-816.
6. Yang, B., D.M. Willies, and C.E. Wyman, *Changes in the enzymatic hydrolysis rate of Avicel cellulose with conversion.* Biotechnology and bioengineering, 2006. **94**(6): p. 1122-1128.
7. Forster, A.V., L.E. Martz, and D.E. Leng, *Process for separating and recovering concentrated hydrochloric acid from the crude product obtained from the acid hydrolysis of cellulose*. 1980, Google Patents.
8. Sathitsuksanoh, N., A. George, and Y.H.P. Zhang, *New lignocellulose pretreatments using cellulose solvents: a review.* Journal of Chemical Technology & Biotechnology, 2013. **88**(2): p. 169-180.
9. Huang, Y.-B. and Y. Fu, *Hydrolysis of cellulose to glucose by solid acid catalysts.* Green Chemistry, 2013. **15**(5): p. 1095-1111.
10. Onda, A., T. Ochi, and K. Yanagisawa, *Selective hydrolysis of cellulose into glucose over solid acid catalysts.* Green Chemistry, 2008. **10**(10): p. 1033-1037.
11. Hu, L., et al., *Chemocatalytic hydrolysis of cellulose into glucose over solid acid catalysts.* Applied Catalysis B: Environmental, 2015. **174**: p. 225-243.
12. Chen, G., et al., *Insights into deactivation mechanism of sulfonated carbonaceous solid acids probed by cellulose hydrolysis.* Catalysis Today, 2019. **319**: p. 25-30.
13. Shuai, L. and X. Pan, *Hydrolysis of cellulose by cellulase-mimetic solid catalyst.* Energy & Environmental Science, 2012. **5**(5): p. 6889-6894.
14. Yang, Q. and X. Pan, *Synthesis and application of bifunctional porous polymers bearing chloride and sulfonic acid as cellulase-mimetic solid acids for cellulose hydrolysis.* BioEnergy Research, 2016. **9**(2): p. 578-586.
15. Tyufekchiev, M., et al., *Cellulase-inspired solid acids for cellulose hydrolysis: structural explanations for high catalytic activity.* ACS Catalysis, 2018. **8**(2): p. 1464-1468.
16. Zhang, Y.H.P. and L.R. Lynd, *Toward an aggregated understanding of enzymatic hydrolysis of cellulose: noncomplexed cellulase systems.* Biotechnology and bioengineering, 2004. **88**(7): p. 797-824.
17. Vanhatalo, K.M. and O.P. Dahl, *Effect of mild acid hydrolysis parameters on properties of microcrystalline cellulose.* BioResources, 2014. **9**(3): p. 4729-4740.
18. Israelachvili, J.N., *Intermolecular and surface forces*. 2011: Academic press.

19. Merk, V., et al., *In situ non-DLVO stabilization of surfactant-free, plasmonic gold nanoparticles: Effect of Hofmeister's anions.* Langmuir, 2014. **30**(15): p. 4213-4222.
20. Ninham, B.W., *On progress in forces since the DLVO theory.* Advances in colloid and interface science, 1999. **83**(1-3): p. 1-17.
21. Van Oss, C.J., M.K. Chaudhury, and R.J. Good, *Interfacial Lifshitz-van der Waals and polar interactions in macroscopic systems.* Chemical reviews, 1988. **88**(6): p. 927-941.
22. Hogg, R., T.W. Healy, and D.W. Fuerstenau, *Mutual coagulation of colloidal dispersions.* Transactions of the Faraday Society, 1966. **62**: p. 1638-1651.
23. Behrens, S.H. and D.G. Grier, *The charge of glass and silica surfaces.* The Journal of Chemical Physics, 2001. **115**(14): p. 6716-6721.
24. Kakiuchi, T., et al., *Double-layer-capacitance titration of self-assembled monolayers of ω-functionalized alkanethiols on Au (111) surface.* Langmuir, 2000. **16**(12): p. 5397-5401.
25. Russel, W.B., et al., *Colloidal dispersions*. 1991: Cambridge university press.
26. Marx, D., *Proton transfer 200 years after von Grotthuss: Insights from ab initio simulations.* ChemPhysChem, 2006. **7**(9): p. 1848-1870.
27. Tadros, T., *Chapter 2 - Colloid and interface aspects of pharmaceutical science*, in *Colloid and Interface Science in Pharmaceutical Research and Development*, H. Ohshima and K. Makino, Editors. 2014, Elsevier: Amsterdam. p. 29-54.
28. Prathapan, R., et al., *Modulating the zeta potential of cellulose nanocrystals using salts and surfactants.* Colloids and Surfaces A: Physicochemical and Engineering Aspects, 2016. **509**: p. 11-18.
29. Heister, E., et al., *Higher dispersion efficacy of functionalized carbon nanotubes in chemical and biological environments.* ACS nano, 2010. **4**(5): p. 2615-2626.
30. Chen, K., et al., *Removal of cadmium and lead ions from water by sulfonated magnetic nanoparticle adsorbents.* Journal of colloid and interface science, 2017. **494**: p. 307-316.
31. Hanaor, D., et al., *The effects of carboxylic acids on the aqueous dispersion and electrophoretic deposition of ZrO2.* Journal of the European Ceramic Society, 2012. **32**(1): p. 235-244.
32. Lu, Z., et al., *Monodisperse magnetizable silica composite particles from heteroaggregate of carboxylic polystyrene latex and Fe3O4 nanoparticles.* Nanotechnology, 2008. **19**(5): p. 055602.
33. Barbati, A.C. and B.J. Kirby, *Electrokinetic measurements of thin Nafion films.* Langmuir, 2014. **30**(8): p. 1985-1993.
34. Qiu, M., et al., *Efficient mechanochemical-assisted production of glucose from cellulose in aqueous solutions by carbonaceous solid acid catalysts.* ACS Sustainable Chemistry & Engineering, 2018. **6**(11): p. 13826-13833.
35. García-García, S., M. Jonsson, and S. Wold, *Temperature effect on the stability of bentonite colloids in water.* Journal of Colloid and Interface Science, 2006. **298**(2): p. 694-705.
36. Wang, D., et al., *A novel acid–base bifunctional catalyst (ZSM-5@ Mg 3 Si 4 O 9 (OH) 4) with core/shell hierarchical structure and superior activities in tandem reactions.* Chemical Communications, 2016. **52**(87): p. 12817-12820.
37. Wakchaure, V.N. and B. List, *A new structural motif for bifunctional Brønsted acid/base organocatalysis.* Angewandte Chemie International Edition, 2010. **49**(24): p. 4136-4139.
38. Robinson, A.M., J.E. Hensley, and J.W. Medlin, *Bifunctional catalysts for upgrading of biomass-derived oxygenates: a review.* ACS catalysis, 2016. **6**(8): p. 5026-5043.
39. Li, H., et al., *Efficient valorization of biomass to biofuels with bifunctional solid catalytic materials.* Progress in Energy and Combustion Science, 2016. **55**: p. 98-194.
40. Song, Y., et al., *Alkaline hydrolysis and flocculation properties of acrylamide-modified cellulose polyelectrolytes.* Carbohydrate polymers, 2011. **86**(1): p. 171-176.
41. Mei, Y., et al., *Catalytic activity of palladium nanoparticles encapsulated in spherical polyelectrolyte brushes and core–shell microgels.* Chemistry of Materials, 2007. **19**(5): p. 1062-1069.
42. Hubbe, M.A., *Flocculation and redispersion of cellulosic fiber suspensions: A review of effects of hydrodynamic shear and polyelectrolytes.* BioResources, 2007. **2**(2): p. 296-331.
43. Ishida, K., et al., *Hydrolysis of cellulose to produce glucose with solid acid catalysts in 1-butyl-3-methyl-imidazolium chloride ([bmIm][Cl]) with sequential water addition.* Biomass Conversion and Biorefinery, 2014. **4**(4): p. 323-331.
44. Li, J. and X. Liang, *Magnetic solid acid catalyst for biodiesel synthesis from waste oil.* Energy Conversion and Management, 2017. **141**: p. 126-132.
45. Zoppe, J.O., et al., *Surface interaction forces of cellulose nanocrystals grafted with thermoresponsive polymer brushes.* Biomacromolecules, 2011. **12**(7): p. 2788-2796.
46. Rehfeldt, F. and M. Tanaka, *Hydration forces in ultrathin films of cellulose.* Langmuir, 2003. **19**(5): p. 1467-1473.
47. Zaccone, A., et al., *Theory of activated-rate processes under shear with application to shear-induced aggregation of colloids.* Physical Review E, 2009. **80**(5): p. 051404.
48. Yan, S., et al., *Mechanochemical Preparation of a H3PO4-Based Solid Catalyst for Heterogeneous Hydrolysis of Cellulose.* ACS omega, 2020. **5**(46): p. 29971-29977.
49. Yamaguchi, D., et al., *Hydrolysis of cellulose by a solid acid catalyst under optimal reaction conditions.* The Journal of Physical Chemistry C, 2009. **113**(8): p. 3181-3188.
50. Liu, W.-J., et al., *Facile synthesis of highly efficient and recyclable magnetic solid acid from biomass waste.* Scientific reports, 2013. **3**(1): p. 1-7.
51. Vancleef, A., et al., *Reducing the induction time using ultrasound and high-shear mixing in a continuous crystallization process.* Crystals, 2018. **8**(8): p. 326.
52. Zinadini, S., et al., *High frequency ultrasound-induced sequence batch reactor as a practical solution for high rate wastewater treatment.* Journal of Environmental Chemical Engineering, 2015. **3**(1): p. 217-226.
53. Sánchez-Cantú, M., et al., *Biodiesel production under mild reaction conditions assisted by high shear mixing.* Renewable Energy, 2019. **130**: p. 174-181.
54. Antonopoulou, E., et al., *Numerical and experimental analysis of the sedimentation of spherical colloidal suspensions under centrifugal force.* Physics of Fluids, 2018. **30**(3): p. 030702.

55. Mohammadi, M., et al., *Brownian dynamics simulations of coagulation of dilute uniform and anisotropic particles under shear flow spanning low to high peclet numbers.* The Journal of chemical physics, 2015. **142**(2): p. 024108.
56. Wan, J. and T. Tokunaga, *Kinetic stability of hematite nanoparticles: the effect ofparticle sizes*. 2006, Ernest Orlando Lawrence Berkeley NationalLaboratory, Berkeley, CA (US).
57. He, Y.T., J. Wan, and T. Tokunaga, *Kinetic stability of hematite nanoparticles: the effect of particle sizes.* Journal of nanoparticle research, 2008. **10**(2): p. 321-332.
58. Aguirre-Pe, J., M.ı.a.L. Olivero, and A.T. Moncada, *Particle densimetric Froude number for estimating sediment transport.* Journal of Hydraulic Engineering, 2003. **129**(6): p. 428-437.